

Stochastic interactions of two Brownian hard spheres in the presence of depletants

Mehdi Karzar-Jeddi, Remco Tuinier, Takashi Taniguchi, and Tai-Hsi Fan

Citation: *The Journal of Chemical Physics* **140**, 214906 (2014); doi: 10.1063/1.4880199

View online: <http://dx.doi.org/10.1063/1.4880199>

View Table of Contents: <http://scitation.aip.org/content/aip/journal/jcp/140/21?ver=pdfcov>

Published by the [AIP Publishing](#)

Articles you may be interested in

[The Newtonian viscosity of concentrated stabilized dispersions: Comparisons with the hard sphere fluid](#)
J. Rheol. **48**, 223 (2004); 10.1122/1.1634986

[Stochastic simulations of DNA in flow: Dynamics and the effects of hydrodynamic interactions](#)
J. Chem. Phys. **116**, 7752 (2002); 10.1063/1.1466831

[Brownian dynamics simulation of the motion of a rigid sphere in a viscous fluid very near a wall](#)
J. Chem. Phys. **113**, 9268 (2000); 10.1063/1.1320829

[Variance reduced Brownian simulation of a bead-spring chain under steady shear flow considering hydrodynamic interaction effects](#)
J. Chem. Phys. **113**, 4767 (2000); 10.1063/1.1288803

[Brownian dynamics simulations on hard-sphere colloidal suspensions](#)
AIP Conf. Proc. **519**, 265 (2000); 10.1063/1.1291567



Stochastic interactions of two Brownian hard spheres in the presence of depletants

Mehdi Karzar-Jeddi,¹ Remco Tuinier,^{2,3} Takashi Taniguchi,⁴ and Tai-Hsi Fan^{1,a)}

¹Department of Mechanical Engineering, University of Connecticut, Storrs, Connecticut 06269-3139, USA

²Van't Hoff Laboratory for Physical and Colloid Chemistry, Debye Institute, Department of Chemistry, Utrecht University, Padualaan 8, 3584 CH, Utrecht, The Netherlands

³DSM ChemTech R&D, P.O. Box 18, 6160 MD Geleen, The Netherlands

⁴Graduate School of Engineering, Kyoto University Katsura Campus, Nishikyo-ku, Kyoto 615-8510, Japan

(Received 3 February 2014; accepted 6 May 2014; published online 6 June 2014)

A quantitative analysis is presented for the stochastic interactions of a pair of Brownian hard spheres in non-adsorbing polymer solutions. The hard spheres are hypothetically trapped by optical tweezers and allowed for random motion near the trapped positions. The investigation focuses on the long-time correlated Brownian motion. The mobility tensor altered by the polymer depletion effect is computed by the boundary integral method, and the corresponding random displacement is determined by the fluctuation-dissipation theorem. From our computations it follows that the presence of depletion layers around the hard spheres has a significant effect on the hydrodynamic interactions and particle dynamics as compared to pure solvent and uniform polymer solution cases. The probability distribution functions of random walks of the two interacting hard spheres that are trapped clearly shift due to the polymer depletion effect. The results show that the reduction of the viscosity in the depletion layers around the spheres and the entropic force due to the overlapping of depletion zones have a significant influence on the correlated Brownian interactions. © 2014 AIP Publishing LLC. [<http://dx.doi.org/10.1063/1.4880199>]

I. INTRODUCTION

The interactions between dispersed colloidal particles in solutions containing non-adsorbing polymer chains play an essential role in many phenomena and processes including macromolecular crowding, protein crystallization, food processing, and co- and self-assembly.^{1–5} Adding non-adsorbing polymer chains to a dispersion of colloids effectively induces an attractive potential between the colloidal particles^{6–8} and alters their phase behavior^{9–14} and transport properties.¹⁵ These changes originate from the presence of polymer depletion zones around the colloidal particles. To avoid the reduction of conformation entropy, polymers prefer to stay away from the colloidal surfaces. Hence depletion zones appear around the colloidal particles. Within the depletion zone the polymer concentration is reduced significantly compared to the bulk polymer concentration. The overlap of depletion layers causes an unbalanced osmotic pressure distribution by the polymers around the colloids, first understood by Asakura and Oosawa.^{6,7} The resulting attractive potential's range and depth can be tuned by polymer size, concentration, and solution conditions. In the last few decades many studies on polymer depletion were focused on the equilibrium aspects of colloid-polymer mixtures, primarily on the depletion interaction, the resulting phase behavior, correct inclusion of polymer-polymer interactions, microstructure of the colloid-polymer suspensions, measurement of depletion forces, and scattering properties.^{9, 10, 12, 13, 16, 18–23}

In order to quantify the dynamic effects of a depletion layer, Donath *et al.*²⁴ proposed an approximation for the hydrodynamic friction of a sphere in a non-adsorbing polymer solution by considering a slip boundary condition at the surface of the particle. Tuinier and Taniguchi considered a viscosity profile near the surface that followed the polymer segment density profile and could account for the polymer depletion-induced flow behavior close to a flat interface.²⁵ The translational and rotational motion of a sphere and a pair of spheres through a non-adsorbing polymer were investigated by us using both a simplified two-layer model^{15, 26} and a continuous viscous profile.^{27–29} For the continuous case, the equilibrium distribution of polymers was determined by mean-field theory.³⁰ When two colloidal spheres are suspended in a liquid, they transfer momentum to each other by the hydrodynamic interactions and hence their stochastic motion is correlated. A way to directly measure the interactions between colloidal particles is to hold the particles in a desired separation distance which can be done by applying an optical trap, first introduced by Ashkin *et al.*³¹ This optical tweezer method has been used to measure the pair interactions under charge stabilization³² and the attractive entropic effect.^{16, 17} Crocker³³ developed a blinking optical trap to measure the free diffusive motion of pair particles. Two spherical particles were brought into a desired separation distance when the tweezer is on, while particles start to diffuse freely when off. The cross-correlation analysis of hydrodynamic interactions of two particles was investigated using optical tweezers.^{34–36} The method has been extended to investigate the dynamics of optically bounded particles³⁷ and the shear effect.^{38, 39} The higher-order effect of the analytical

^{a)} Author to whom correspondence should be addressed. Electronic mail: thfan@enr.uconn.edu

mobility tensor for pair particles in a homogeneous fluid was investigated by He *et al.*⁴⁰

There is a strong need in theoretically quantifying the polymer depletion effect on the stochastic interactions of a pair of colloidal particles. Here we present the results of the mobility functions of two interacting spheres and the thermodynamic potential due to the entropic effect. The self- and cross-correlation of the pair particles' random displacements under dilute to semi-dilute polymer solution conditions are compared to pure solvent case. When accounting for polymer, the polymer entanglement is neglected and the fluid flow is assumed Newtonian. Background polymer fluctuations are also not considered here. The simplified two-layer continuum model is applied to both hydrodynamic and thermodynamic interactions. The polymer structure relaxation is assumed much faster than the long-time Brownian motion such that the depletion envelop always follows the sphere's trajectory. The mobility is computed deterministically by the boundary integral method, and the result is coupled to the random displacements of the colloidal hard spheres to ensure the consistency of the fluctuation-dissipation theorem.

II. THEORETICAL FORMULATION

We consider Brownian motion of a pair of isotropic and equal-sized hard spheres in a dilute to semi-dilute non-adsorbing polymer solution. It is assumed that each colloidal particle is surrounded by an assumed equilibrium depletion layer. The mean positions of both hard spheres are fixed by the optical traps as illustrated in Fig. 1. The depletion zone around each sphere is represented by the simplified two-layer model¹⁵ that has uniform solvent viscosity (η_s) in the inner layer (Ω_s) and uniform bulk polymer solution viscosity (η_p) in the bulk (Ω_p).

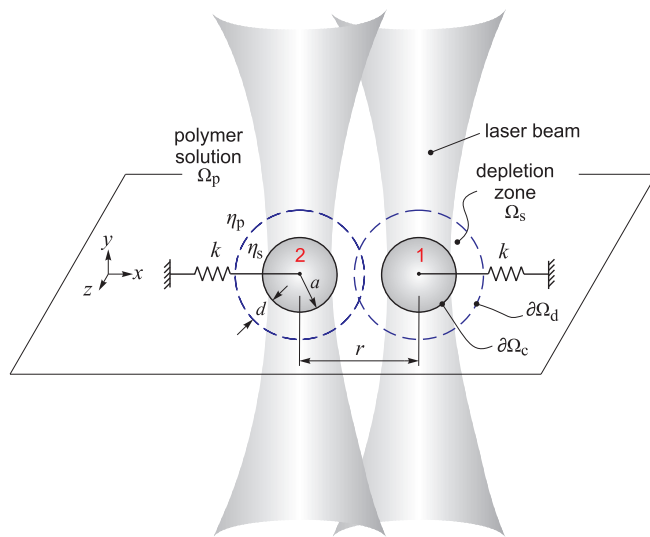


FIG. 1. Schematic of a pair of interacting colloidal spheres located by optical tweezers. The domains Ω_p and Ω_s are for the bulk solution and the polymer depletion zones, respectively. η_p and η_s are the corresponding bulk and solvent viscosities. The distance d is the apparent thickness of the depletion layer, a is colloid radius, and k is the stiffness that represents the trapping potential. The particle tags 1 and 2 are given.

A. Two-layer model

In the bulk solution, the polymer solution viscosity can be approximated by the Martin equation,⁴¹

$$\lambda = \frac{\eta_p}{\eta_s} = 1 + [\eta]c_b e^{k_H[\eta]c_b} = 1 + \epsilon e^{k_H\epsilon}, \quad (1)$$

where η_p and η_s are the corresponding bulk and solvent viscosities, respectively, c_b is the bulk polymer concentration, $[\eta] = 1/c_b^*$ is the intrinsic viscosity of the polymer, c_b^* is the polymer overlap concentration, and k_H is the Huggins coefficient. For the polymer concentration we use the scaled quantity $\epsilon = [\eta]c_b = c_b/c_b^*$.

The depletion thickness around the hard spheres can be calculated based on the bulk concentration and the sizes of the polymers and colloid spheres. As a correction of the depletion thickness at a planar surface d_p ,³⁰ the thickness at a spherical surface can be expressed as

$$d = a \left[1 + 3\frac{d_p}{a} + \frac{\pi^2}{4} \left(\frac{d_p}{a} \right)^2 \right]^{1/3} - a, \quad (2)$$

where d_p is the depletion thickness for a planar surface, a is the colloid radius, $d_p \simeq d_0\sqrt{1/(1+c_1\epsilon^2)}$, where $d_0 = 2R_g/\sqrt{\pi}$ indicates the thickness in the dilute limit, and R_g is the radius of gyration of polymers. The coefficient c_1 is around 6.02 for polymers in a theta solvent, and in a good solvent $d_p \simeq d_0\sqrt{1/(1+c_1\epsilon^{1.54})}$ and $c_1 \simeq 3.95$.^{14,30}

According to the Asakura-Oosawa (AO) theory and Vrij's penetrable hard sphere model,^{6,8} the depletion potential between two hard spheres in a solution of dilute depletants is given by the product of the osmotic pressure Π and the overlap volume of the polymer depletion zones,⁸

$$W^{\text{dep}}(\epsilon, r) = \begin{cases} \infty & \text{for } r \leq 2a \\ -\frac{4\pi}{3}(a+d)^3 \left[1 - \frac{3}{4} \left(\frac{r}{a+d} \right) + \frac{1}{16} \left(\frac{r}{a+d} \right)^3 \right] \Pi(\epsilon) & \text{for } 2a < r \leq 2(a+d) \\ 0 & \text{for } r > 2(a+d), \end{cases} \quad (3)$$

where $r = |\mathbf{r}_1 - \mathbf{r}_2|$ is the center-to-center distance of the hard spheres, $\Pi(\epsilon) = \Pi_0[1 + c_2\epsilon^2]$ approximates the osmotic pressure in the dilute to semi-dilute regime,¹⁴ where $\Pi_0(\epsilon) = n_b(\epsilon)k_B T$ is for the dilute limit with $n_b(\epsilon) = 3\epsilon/(4\pi R_g^3)$ as the number density of polymers, and c_2 is around 4.1 for a theta solvent.¹⁴ In a good solvent, $\Pi(\epsilon) \simeq \Pi_0[1 + c_2\epsilon^{1.31}]$ and $c_2 \simeq 1.62$. The corresponding depletion force therefore is

$$\mathbf{F}_\alpha^{\text{dep}}(\epsilon, r) = -\nabla W^{\text{dep}}(\epsilon, r) = \pi(a+d)^2 \left[1 - \frac{1}{4} \left(\frac{r}{a+d} \right)^2 \right] \Pi(\epsilon) \hat{\mathbf{r}}_{\alpha\beta} \quad (4)$$

for $2a < r \leq 2(a+d)$, where $\hat{\mathbf{r}}_{\alpha\beta} = [\mathbf{r}_\beta - \mathbf{r}_\alpha]/r$ is the unit vector pointing from particle α to β .

B. Brownian interactions

The translational Brownian motions of both spheres in two quiescent fluid can be described by the general Langevin equation,⁴²

$$m_{\alpha} \ddot{\mathbf{r}}_{\alpha} = \mathbf{F}_{\alpha}^{\text{H}} + \mathbf{F}_{\alpha}^{\text{P}} + \mathbf{F}_{\alpha}^{\text{B}} \quad (\alpha = 1, 2), \quad (5)$$

where m is the particle mass, α labels particles 1 and 2, \mathbf{r} is the particle position vector, and the force summation acting on the hard spheres includes contributions of hydrodynamic forces ($\mathbf{F}_{\alpha}^{\text{H}}$), polymer depletion and optical trapping forces (non-hydrodynamic, $\mathbf{F}_{\alpha}^{\text{P}}$), and the random thermal fluctuation force ($\mathbf{F}_{\alpha}^{\text{B}}$) that drives the Brownian motion. They can be written as

$$\mathbf{F}_{\alpha}^{\text{H}} = -(\zeta_{\alpha 1} \cdot \dot{\mathbf{r}}_1 + \zeta_{\alpha 2} \cdot \dot{\mathbf{r}}_2), \quad (6)$$

$$\mathbf{F}_{\alpha}^{\text{P}} = \mathbf{F}_{\alpha}^{\text{dep}} + \mathbf{F}_{\alpha}^{\text{trap}}, \quad (7)$$

and

$$\mathbf{F}_{\alpha}^{\text{B}} = \kappa_{\alpha 1} \cdot \mathbf{x}_1 + \kappa_{\alpha 2} \cdot \mathbf{x}_2, \quad (8)$$

where ζ is the resistance tensor, κ is the weighting coefficient tensor, and the vector \mathbf{x} contains random numbers in Cartesian coordinates and is defined by a Gaussian distribution with mean $\langle \mathbf{x}_{\alpha}(t) \rangle = \mathbf{0}$ and co-variance $\langle \mathbf{x}_{\alpha}(t) \mathbf{x}_{\beta}(t + t') \rangle = 2\delta_{\alpha\beta} \delta(t') \mathbf{I}$, where δ is the Kronecker delta, \mathbf{I} is the identity tensor, and $\alpha, \beta = 1, 2$. The coefficient κ is related to the thermal energy $k_{\text{B}}T$ and the resistance tensor ζ through the fluctuation-dissipation theory,⁴³

$$\zeta_{\alpha\beta} = \frac{1}{k_{\text{B}}T} (\kappa_{\alpha 1} \cdot \kappa_{1\beta} + \kappa_{\alpha 2} \cdot \kappa_{2\beta}) \quad (\alpha, \beta = 1, 2). \quad (9)$$

The non-hydrodynamic force includes the entropic and optical trapping forces. For a small displacement away from the equilibrium position of the hard spheres, the optical trap provides a three-dimensional harmonic force,⁴⁴

$$\mathbf{F}_{\alpha}^{\text{trap}} = -k [\mathbf{r}_{\alpha}(t) - \mathbf{r}_{\alpha}^0], \quad (10)$$

where k is the apparent stiffness of the potential, and the superscript 0 indicates the equilibrium position in absence of the depletion potential. The stiffness of the harmonic force is approximately a linear function of the light intensity.⁴⁴

In order to quantify typical time scales we consider colloidal spheres with radius 500 nm in an optical trap with a stiffness of 18.5 pN/ μm ³⁴ in an aqueous solvent. The characteristic relaxation time for the colloidal Brownian motion under the potential can then be estimated by $6\pi\eta_s a/k \simeq 10^{-3}$ s. If the mass density of the colloid is similar to solvent, the momentum relaxation or decorrelation time, $m/6\pi\eta_s a$, is about 10^{-7} s, where η_s is the solvent viscosity. The diffusive time scale for the colloid over its radius is $\sim 6\pi\eta_s a^3/k_{\text{B}}T \simeq 0.6$ s. Therefore, for the long-time diffusive interaction, the motion of hard spheres is overdamped and the inertial effect is assumed negligible. By integrating the quasi-steady Langevin equation the new position for the colloidal sphere α at each simulation time step (\gg momentum decorrelation time) can be described by the following diffusive displacement

equation,⁴⁵

$$\begin{aligned} \mathbf{r}_{\alpha}(t + \Delta t) &= \mathbf{r}_{\alpha}(t) + \left[\frac{\partial}{\partial \mathbf{r}_1(t)} \cdot \mathbf{D}_{\alpha 1}(t) + \frac{\partial}{\partial \mathbf{r}_2(t)} \cdot \mathbf{D}_{\alpha 2}(t) \right] \Delta t \\ &+ \frac{1}{k_{\text{B}}T} [\mathbf{D}_{\alpha 1}(t) \cdot \mathbf{F}_1^{\text{P}}(t) + \mathbf{D}_{\alpha 2}(t) \cdot \mathbf{F}_2^{\text{P}}(t)] \Delta t + \mathbf{R}_{\alpha}(\Delta t), \end{aligned} \quad (11)$$

where $\mathbf{D}_{\alpha\beta}$ ($\alpha, \beta = 1, 2$) is the diffusion tensor, Δt is the integration time step, and \mathbf{R}_{α} is the random displacement that has zero mean $\langle \mathbf{R}_{\alpha}(\Delta t) \rangle = \mathbf{0}$, and covariance $\langle \mathbf{R}_{\alpha}(\Delta t) \mathbf{R}_{\beta}(\Delta t) \rangle = 2\mathbf{D}_{\alpha\beta}(t) \Delta t$. The displacements resulting from the spatial variation of the diffusion tensor, the potential forces acting on both hard spheres, and the thermal fluctuation are all included in the formulation. Computationally, the random displacement vector can be determined by $R_i(\Delta t) = \sum_{j=1}^i L_{ij}(\mathbf{D}_{\alpha\beta}) X_j(\Delta t)$ ($i = 1, 2, \dots, 6$), where $i = 1, 2, 3$ represent Cartesian components for colloid $\alpha = 1$, and $i = 4, 5, 6$ are components for colloid $\alpha = 2$, tensor L is the weighting factor for random displacement, $\mathbf{L}_{\alpha\beta} = (\mathbf{D}_{\alpha 1} \cdot \kappa_{1\beta} + \mathbf{D}_{\alpha 2} \cdot \kappa_{2\beta})/k_{\text{B}}T$, and X_1, X_2, \dots, X_6 are series of random variables with zero mean and a covariance of $\sqrt{2\Delta t}$.⁴⁵

C. Mobility functions

Since we apply the two layer approach to account for the depletion zones, the Rotne-Prager tensors⁴⁶ or higher-order corrections⁴⁷ are not applicable for resolving the self- and mutual-diffusivity. The diffusivity $\mathbf{D}_{\alpha\beta} = k_{\text{B}}T \zeta_{\alpha\beta}^{-1}$ here is quantified based on the distance between the hard spheres (r), the thickness of polymer depletion layer (d), and the bulk-to-solvent viscosity ratio ($\lambda = \eta_{\text{p}}/\eta_{\text{s}}$). The self-diffusivity can be formulated as a correction of the mobility functions^{47,48} for the motion of a pair of spheres in a homogeneous medium,

$$\begin{aligned} \mathbf{D}_{\alpha\alpha}(r, d, \lambda) &= \frac{D_0}{g_0(d, \lambda)} [\mathbf{I} + A^{\text{s}}(r, d, \lambda) \hat{\mathbf{r}}_{\alpha\beta} \hat{\mathbf{r}}_{\alpha\beta} \\ &+ B^{\text{s}}(r, d, \lambda) (\mathbf{I} - \hat{\mathbf{r}}_{\alpha\beta} \hat{\mathbf{r}}_{\alpha\beta})], \end{aligned} \quad (12)$$

where $\alpha, \beta = 1, 2$ and $\alpha \neq \beta$, $g_0(d, \lambda)$ is the correction factor for the hydrodynamic friction coefficient of an isolated hard sphere $6\pi\eta_s a$ due to the depletion layer,²⁶ $D_0 = k_{\text{B}}T/6\pi\eta_s a$ is the diffusivity of an isolated sphere in a pure solvent, \mathbf{I} is the identity matrix, A and B are mobility functions in parallel and perpendicular directions, respectively, and the superscript s is for self-mobility. Throughout this paper the correction factor g with any super- and sub-script describes the deviation of the friction from a single sphere in a pure solvent (for which $g = 1$). Similarly, the mutual diffusivity can be expressed as

$$\begin{aligned} \mathbf{D}_{\alpha\beta}(r, d, \lambda) &= \frac{D_0}{g_0(d, \lambda)} [A^{\text{c}}(r, d, \lambda) \hat{\mathbf{r}}_{\alpha\beta} \hat{\mathbf{r}}_{\alpha\beta} \\ &+ B^{\text{c}}(r, d, \lambda) (\mathbf{I} - \hat{\mathbf{r}}_{\alpha\beta} \hat{\mathbf{r}}_{\alpha\beta})], \end{aligned} \quad (13)$$

where $\alpha, \beta = 1, 2$ and $\alpha \neq \beta$, the superscript c indicates cross-mobility. The analytical expression for a single particle based on the two-layer approximation is given by²⁶

$$g_0(d, \lambda) = \frac{2}{\Gamma} [(2 + 3\lambda^{-1})(1 + d^*)^6 - 2(1 - \lambda^{-1})(1 + d^*)], \quad (14)$$

where $d^* = d/a$ is the normalized depletion thickness and

$$\Gamma = 2(2 + 3\lambda^{-1})(1 + d^*)^6 - 3(3 + 2\lambda^{-1})(1 - \lambda^{-1})(1 + d^*)^5 + 10(1 - \lambda^{-1})(1 + d^*)^3 - 9(1 - \lambda^{-1})(1 + d^*) + 4(1 - \lambda^{-1})^2. \quad (15)$$

Here the mobility functions are decoupled and computed by the boundary integral method. Specifically, the four functions are expressed as

$$\begin{aligned} A^s(r, d, \lambda) &= \frac{g_0(d, \lambda)}{2} \left[\frac{1}{g_{\parallel}^I(r, d, \lambda)} + \frac{1}{g_{\parallel}^{II}(r, d, \lambda)} \right] - 1, \\ B^s(r, d, \lambda) &= \frac{g_0(d, \lambda)}{2} \left[\frac{1}{g_{\perp}^I(r, d, \lambda)} + \frac{1}{g_{\perp}^{II}(r, d, \lambda)} \right] - 1, \\ A^c(r, d, \lambda) &= \frac{g_0(d, \lambda)}{2} \left[\frac{1}{g_{\parallel}^I(r, d, \lambda)} + \frac{-1}{g_{\parallel}^{II}(r, d, \lambda)} \right], \quad \text{and} \\ B^c(r, d, \lambda) &= \frac{g_0(d, \lambda)}{2} \left[\frac{1}{g_{\perp}^I(r, d, \lambda)} + \frac{-1}{g_{\perp}^{II}(r, d, \lambda)} \right], \end{aligned} \quad (16)$$

where g_{\parallel}^I , g_{\parallel}^{II} , g_{\perp}^I , and g_{\perp}^{II} are the corrections or the scaled resistances due to depletion effect and the hydrodynamic interaction between both spheres, defined as

$$\begin{aligned} g_{\parallel}^I(r, d, \lambda) &= \frac{F_{\parallel}^I(r, d, \lambda)}{6\pi\eta_s a U}, \quad g_{\parallel}^{II} = \frac{F_{\parallel}^{II}}{6\pi\eta_s a U}, \\ g_{\perp}^I &= \frac{F_{\perp}^I}{6\pi\eta_s a U}, \quad \text{and} \quad g_{\perp}^{II} = \frac{F_{\perp}^{II}}{6\pi\eta_s a U}, \end{aligned} \quad (17)$$

where the four hydrodynamic interaction modes F_{\parallel}^I , F_{\parallel}^{II} , F_{\perp}^I , and F_{\perp}^{II} (see Fig. 4 in Sec. III) are the computed resistance on each sphere for the interaction parallel and perpendicular to the center-to-center line, respectively. U is the velocity magnitude of both colloids, and $g \rightarrow 1$ as $r \rightarrow \infty$. For mode I (indicated by the superscript) both spheres move in the same direction, whereas in mode II both spheres move in the opposite direction. Accordingly, the divergence of the diffusivity tensor becomes (the Appendix)

$$\begin{aligned} \frac{\partial}{\partial \mathbf{r}_1} \cdot \mathbf{D}_{11}(r, d, \lambda) &= \frac{-D_0}{g_0} \left[\frac{\partial A^s}{\partial r} + \frac{2(A^s - B^s)}{r} \right] \hat{\mathbf{r}}_{12} \\ &= -\frac{\partial}{\partial \mathbf{r}_2} \cdot \mathbf{D}_{22}, \end{aligned} \quad (18)$$

and

$$\begin{aligned} \frac{\partial}{\partial \mathbf{r}_2} \cdot \mathbf{D}_{12}(r, d, \lambda) &= \frac{D_0}{g_0} \left[\frac{\partial A^c}{\partial r} + \frac{2(A^c - B^c)}{r} \right] \hat{\mathbf{r}}_{12} \\ &= -\frac{\partial}{\partial \mathbf{r}_1} \cdot \mathbf{D}_{21}. \end{aligned} \quad (19)$$

For a pair of hard spheres moving in a pure solvent the analytical approximation for all modes of hydrodynamic interactions have been provided by Stimson and Jeffery,⁴⁹

Brenner,⁵⁰ and O'Neill.⁵¹ However, the analytical results that account for the polymer depletion effect on pair interaction are not available. Here we apply the boundary integral method to compute the hydrodynamic interactions, i.e., F_{\parallel}^I , F_{\parallel}^{II} , F_{\perp}^I , and F_{\perp}^{II} in order to determine the random displacements that are consistent with the fluctuation-dissipation theorem.

D. Integral formulation of the pair hydrodynamic interaction

The quasi-steady Stokes flow applied to the two-layer model can be formulated as

$$\eta_p \nabla^2 \mathbf{v}^{(p)} - \nabla p^{(p)} = 0, \quad \nabla \cdot \mathbf{v}^{(p)} = 0 \quad \text{for } \mathbf{r} \in \Omega_p, \quad (20)$$

and

$$\eta_s \nabla^2 \mathbf{v}^{(s)} - \nabla p^{(s)} = 0, \quad \nabla \cdot \mathbf{v}^{(s)} = 0 \quad \text{for } \mathbf{r} \in \Omega_s, \quad (21)$$

where \mathbf{v} is velocity, p is pressure, \mathbf{r} is position vector, superscript s and p indicate the solvent (depletion zone) and bulk polymer solution, respectively. The no-slip boundary condition is applied at the particle surface by combining the translational and rotational velocity, $\mathbf{v}^{(s)} = \mathbf{U}_\alpha + \boldsymbol{\omega}_\alpha \times \boldsymbol{\ell}_\alpha$ ($\alpha = 1, 2$). The far-field boundary conditions are $\mathbf{v}^{(p)} \rightarrow \mathbf{0}$ and $p^{(p)} \rightarrow p^\infty$ as $\mathbf{r} \rightarrow \infty$. At the interface between the depletion zone and the bulk polymer solution, the velocity and stress are continuous, i.e., $\mathbf{v}^{(s)} = \mathbf{v}^{(p)}$, and $\boldsymbol{\tau}^{(s)} = \boldsymbol{\tau}^{(p)}$ presuming that the surface tension at the interface is negligible. The translation velocity for four interactive modes is defined as

$$\begin{aligned} \parallel \text{ mode I : } \mathbf{U}_1 &= \mathbf{U}_2 = U_0 \hat{\mathbf{e}}_x, \\ \parallel \text{ mode II : } \mathbf{U}_1 &= -\mathbf{U}_2 = -U_0 \hat{\mathbf{e}}_x, \\ \perp \text{ mode I : } \mathbf{U}_1 &= \mathbf{U}_2 = U_0 \hat{\mathbf{e}}_z, \quad \text{and} \\ \perp \text{ mode II : } \mathbf{U}_1 &= -\mathbf{U}_2 = -U_0 \hat{\mathbf{e}}_z, \end{aligned} \quad (22)$$

where U_0 is the velocity magnitude and both spheres are aligned along the x -axis. These modes are illustrated by the arrows in the spheres in Fig. 4.

To compute the resistance, the integral formulation of the Stokes flow⁵² is applied for the two-layer model. In the fluid domain Ω bounded by surface $\partial\Omega$, the velocity field satisfies the integral momentum equation, $\int_{\partial\Omega} f_i G_{ij} dS - \eta \int_{\partial\Omega} v_i T_{ijk} n_k dS = 0$ when the source point is located outside the fluid domain, while $v_j = -\int_{\partial\Omega} f_i G_{ij} / (8\pi\eta) dS + \int_{\partial\Omega} v_i T_{ijk} n_k / (8\pi) dS$ when the source point is within the domain. Here η is the viscosity, i and j are Einstein notations, $f_i = \tau_{ij} n_j$ is traction, n represents the surface normal pointing into the fluid, G_{ij} is the fundamental solution (Stokeslet) of the Stokes equation, and T_{ijk} is its corresponding stress field (stresslet), written as

$$G_{ij}(\mathbf{r}, \mathbf{r}_0) = \frac{\delta_{ij}}{x} + \frac{x_i x_j}{x^3}, \quad \text{and} \quad T_{ijk}(\mathbf{r}, \mathbf{r}_0) = -\frac{6x_i x_j x_k}{x^5}, \quad (23)$$

here \mathbf{r}_0 and \mathbf{r} are the source and field points, respectively, $x = |\mathbf{x}|$ and $\mathbf{x} = \mathbf{r} - \mathbf{r}_0$. By applying the integral formulation and incorporating the stress-free condition at the interface between the depletion zone and the bulk solution $\partial\Omega_d$ (Fig. 2),

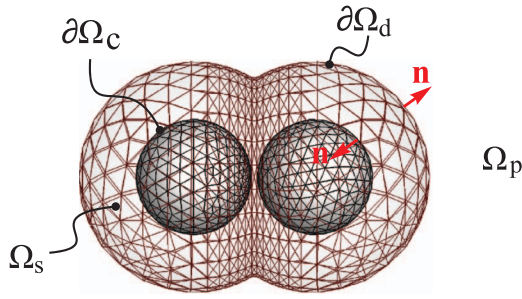


FIG. 2. Illustration of the surface mesh applied to the integral computation. $\partial\Omega_d$ is the interface between the depletion zone and the bulk polymer solution. The mesh is refined near the region of overlapping depletion zones.

$\Delta f_i = f_i^{(p)} - f_i^{(s)} = 0$, we have

$$v_j(\mathbf{r}_0 \in \Omega_p) = \frac{1}{8\pi\eta_p} \int_{\partial\Omega_c} f_i G_{ij} dS - \frac{1}{8\pi\lambda} \int_{\partial\Omega_c} (U_i + \varepsilon_{ijk}\omega_j \ell_k) T_{ijk} n_k dS + \frac{1-1/\lambda}{8\pi} \int_{\partial\Omega_d} v_i T_{ijk} n_k dS \quad (24)$$

and

$$\frac{1}{\lambda} v_j(\mathbf{r}_0 \in \Omega_s) = \frac{1}{8\pi\eta_p} \int_{\partial\Omega_c} f_i G_{ij} dS - \frac{1}{8\pi\lambda} \int_{\partial\Omega_c} (U_i + \varepsilon_{ijk}\omega_j \ell_k) T_{ijk} n_k dS + \frac{1-1/\lambda}{8\pi} \int_{\partial\Omega_d} v_i T_{ijk} n_k dS, \quad (25)$$

where ε_{ijk} is the permutation tensor, and the directions of surface normals are given in Fig. 2. As the source approaches the colloidal surface and the depletion interface, the Cauchy principle value is applied to the double-layer integral that includes the velocity term.⁵³

As a result, the corresponding integral equation can be derived for the two-layer model for the entire computation

domain shown in Fig. 2, expressed as

$$\mathcal{H}v_j(\mathbf{r}_0) = \frac{1}{8\pi\eta_p} \int_{\partial\Omega_c} f_i G_{ij} dS - \frac{1}{8\pi\lambda} \int_{\partial\Omega_c} (U_i + \varepsilon_{ijk}\omega_j \ell_k) T_{ijk} n_k dS + \frac{1-1/\lambda}{8\pi} \int_{\partial\Omega_d} v_i T_{ijk} n_k dS, \quad (26)$$

where coefficient $\mathcal{H} = 1$ for $\mathbf{r}_0 \in \Omega_p$, $\mathcal{H} = 1/\lambda$ for $\mathbf{r}_0 \in \Omega_s$, $\mathcal{H} = (\lambda + 1)/(2\lambda)$ for $\mathbf{r}_0 \in \partial\Omega_d$, and $\mathcal{H} = 1/(2\lambda)$ for $\mathbf{r}_0 \in \partial\Omega_c$. In the integral equation the rotational velocity ω_j is unknown *a priori*. It can be determined by the vanishing torque applied to both isotropic spheres due to the hydrodynamic coupling,

$$\mathcal{T}_\alpha = \int_{\partial\Omega_{c,\alpha}} \varepsilon_{ijk} \ell_j f_k dS = 0. \quad (27)$$

In summary, the integral equations (Eqs. (26) and (27)) are discretized and computed for the primary variables $v_j(\mathbf{r}_0 \in \partial\Omega_d)$, $f_j(\mathbf{r}_0 \in \partial\Omega_c)$, and the rotational velocity for each sphere ω_j . Once the boundary values are found, the results in the fluid domains can be obtained from Eqs. (24) and (25).

III. RESULTS AND DISCUSSION

The stochastic motions of both spheres are correlated due to hydrodynamic and thermodynamic interactions. The four hydrodynamic modes represented by F_{\parallel}^I , F_{\parallel}^{II} , F_{\perp}^I , and F_{\perp}^{II} are functions of the separation distance r , the polymer-to-sphere size ratio, and the polymer concentration. The latter quantity affects the bulk viscosity as well as the strength of the depletion attraction. Here the two-layer model requires two input parameters, the depletion thickness d and the bulk-to-solvent viscosity ratio λ . Figure 3 shows the flow patterns induced by the moving spheres corresponding to two parallel (Figs. 3(a) and 3(b)) and two perpendicular (Figs. 3(c) and 3(d)) modes with respect to the center-to-center line. Patterns 3a' to 3d' are corresponding typical Stokes flow for comparison. In the dilute limit, all flow patterns are similar to the cases in a uniform fluid medium as expected (Figs. 3(a') to 3(d')), while for a higher value of viscosity ratio, e.g., $\lambda = 10$ as shown in

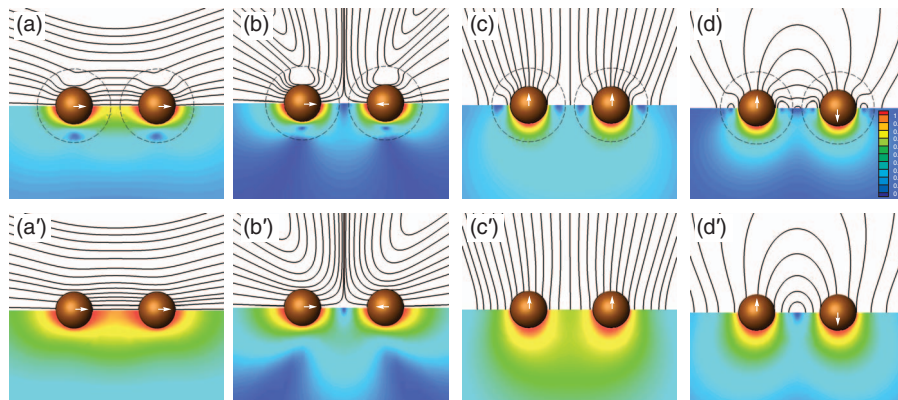


FIG. 3. Streamlines and contours of the normalized velocities around interacting hard spheres in parallel and transverse directions, with (top panels from (a) to (d)) and without ((a') to (d')) polymer depletion zones. Parameters used for the demonstration are: $da = 1$, $ra = 4.5$, and $\lambda = 10$.

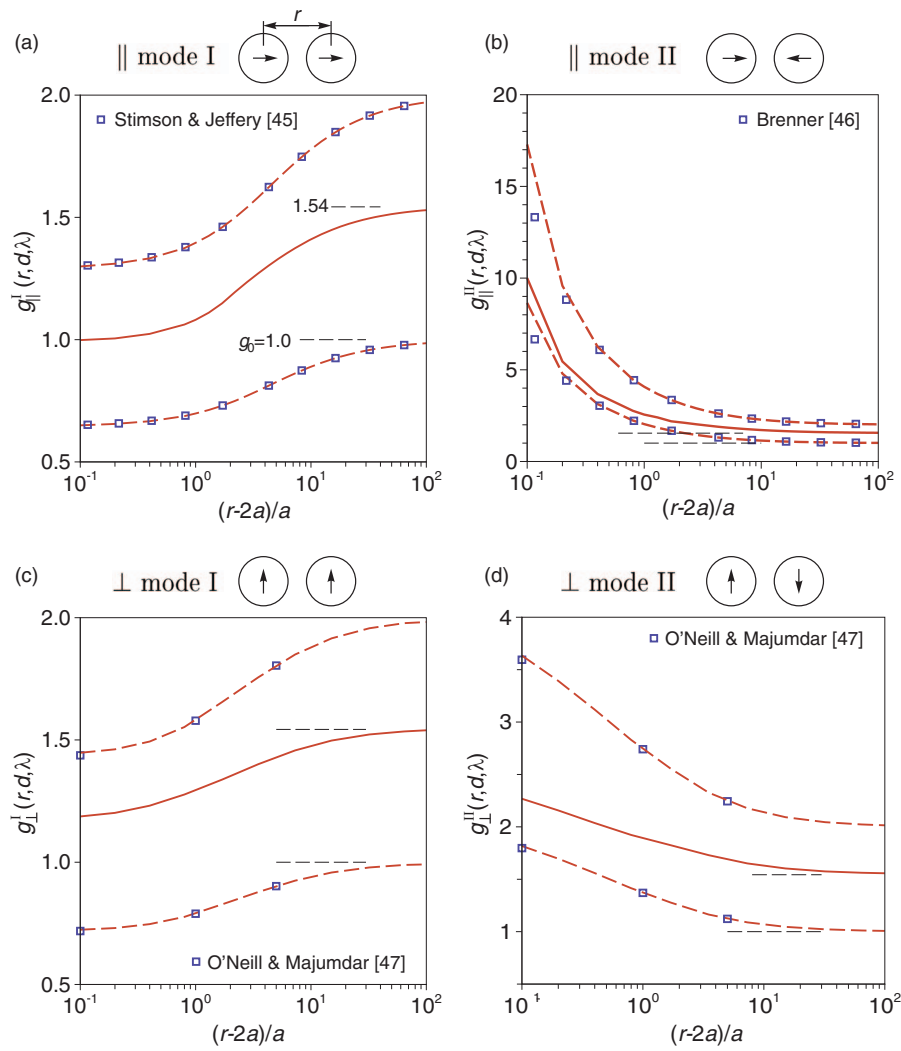


FIG. 4. Semi-log plots showing the hydrodynamic correction function g versus the scaled separation distance for both parallel and perpendicular motions to the center-to-center line along the same (a, c) and opposite (b, d) directions. The square data points are the exact series solution for a uniform solvent (lower bound) and uniform bulk solution (upper bound).^{49–51} The dashed-lines indicate boundary integral results as a numerical validation. The solid curves show the results for hard spheres in a nonadsorbing polymer solution with depletion layer described using the two-layer model.

Figs. 3(b) and 3(d), circulations appear in the depletion zone near the particle surface due to the cage-like behavior, which is similar to what we reported earlier for the single particle.^{15,26} The near-field effect has significant impact on the stress distribution and therefore the overall resistance applied to the spheres. The circulation further complicates the slip-like behavior and changes the shear and normal viscous force near the front and aft surface. The overall slip-like behavior yields a fast decay of the velocity magnitude away from the particle surface. Overall, mode II has a great reduction of the resistance, whereas in mode I the reduction is less significant. As later shown in Fig. 4, the hydrodynamic correction factor approaches the resistance-distance curve dominated by the solvent viscosity (the lower bound) in modes II for both parallel and perpendicular directions.

Figures 4(a) and 4(b) show the correction factors (Eq. (17)) for the hydrodynamic resistance at various scaled separation distance under parallel motion along the same (a) and opposite (b) directions. The boundary integral result is validated by the analytical approximations (the upper and

lower bounds) for mode I⁴⁹ and mode II,⁵⁰ written as

$$g_{||}^I = \frac{4}{3} \sinh(\theta) \sum_{n=1}^{\infty} \frac{n(n+1)}{(2n-1)(2n+3)} \times \left\{ 1 - \frac{4 \sinh^2(n + \frac{1}{2})\theta - (2n+1)^2 \sinh^2 \theta}{2 \sinh(2n+1)\theta + (2n+1) \sinh 2\theta} \right\}, \quad (28)$$

where $\theta = \cosh^{-1}(r/2a)$ and

$$g_{||}^{II} = \frac{4}{3} \sinh(\theta) \sum_{n=1}^{\infty} \frac{n(n+1)}{(2n-1)(2n+3)} \times \left\{ \frac{4 \cosh^2(n + \frac{1}{2})\theta + (2n+1)^2 \sinh^2 \theta}{2 \sinh(2n+1)\theta - (2n+1) \sinh 2\theta} - 1 \right\}. \quad (29)$$

In the presence of the depletants, the hydrodynamic resistance is bounded by two limiting cases: solvent only and uniform polymer solution without the depletion effect (shown by the analytical data points and numerical dashed curves). The solid curve in between the upper and lower bounds

illustrates the numerical results obtained for hard spheres in a non-adsorbing polymer solution described using the two-layer model. The asymptote $g \rightarrow 1.54$ is the analytical result for the resistance of a single sphere under the same depletion condition,²⁶ and $g \rightarrow 1.0$ is the Stokes limit. For the uniform polymer solution the asymptote is $g \rightarrow \lambda=2$ (the upper bound). In the lubrication regime when two spheres are close to each other ($r/a \rightarrow 2$, mode II, Figs. 4(b) and 4(d)), the resistance approaches the solvent limit due to the dominant stress contribution from the polymer-depleted liquid film in between the spheres. However, on mode I (Figs. 4(a) and 4(c)) the thin liquid film has much less influence on the resistance compared with that from the surrounding fluid. The analytical results on the perpendicular modes (square data points in Figs. 4(c) and 4(d)) are provided by O'Neill and Majumdar,⁵¹ which are presented by the lower and upper bounds that we also used to validate the boundary integral results. The three data points are shown in Figs. 4(c) and 4(d). The same asymptotes as presented in the parallel mode are given for large separation distance. Note that in the lubrication limit, the liquid film has less effect on perpendicular-mode II compared with the parallel motion due to the torque-free condition.

In Fig. 5 we compare typical depletion and trapping harmonic potentials applied to the hard spheres. In general, the attractive force is enhanced by a higher polymer concentration if the overlap volume remains the same. However, the depletion thickness reduces as the bulk polymer concentration increases, which reduces the overlap volume and suppresses the attractive force. The value for the stiffness of the optical trap has a significant caging effect on the Brownian motion of both spheres as the simulation results illustrated in Fig. 5(b). Parameters used in the simulation are: time step $\Delta t = 28.5 \mu\text{s}$, radius $a = 500 \text{ nm}$, polymer concentration $\epsilon = 0.5$, and depletion thickness $d/a = 0.69$ that corresponds to $R_g/a = 1$. The distance between the traps and the initial particle separation distance are set to $r/a = 2.5$. Both hydrodynamic and depletion effects are taken into account, the data points clearly shows the attractive depletion effect on the probability

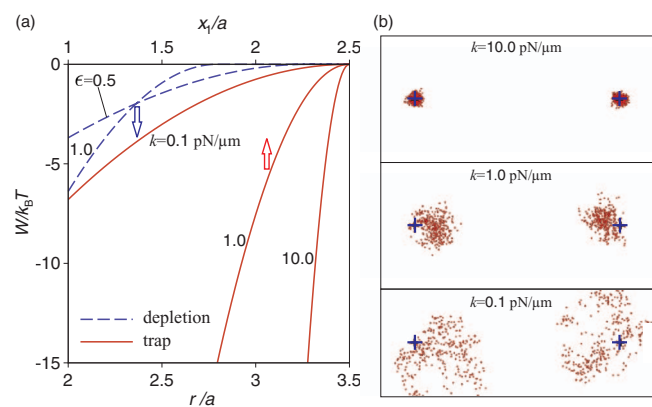


FIG. 5. (a) The comparison of the potential of the optical trap applied to the particle with the trapping center located at $x_1/a = 2.5$ and the polymer depletion potential between two spheres versus the center-to-center separation distance r/a ($=2$ when spheres are in contact with each other). (b) A test run of Brownian simulations with data points showing the particle position per 200 time steps. The total simulation time is 2 s. In this test case, $d/a = 1$ and $\lambda = 2$. The centers of two traps are indicated by the plus signs.

distribution of the spheres, with the characteristic distribution length inversely proportional to the square root of k . Next we consider the correlation analysis that better characterizes the ensemble results.

As a baseline comparison for the correlation analysis, the long-time autocorrelation of the random displacement is considered for a single Brownian sphere with and without polymer depletion, which can be formulated by the analytical result,⁵⁴

$$\langle x(t)x(0) \rangle = \frac{k_B T}{k} \left[\exp\left(-\frac{t}{\tau}\right) \right], \quad (30)$$

where $k_B T/k$ measures the thermal energy versus the strength of the harmonic potential, and more importantly the decorrelation time depends on corrected hydrodynamic resistance and the harmonic potential,

$$\tau = \frac{6\pi\eta_s a g_0(\lambda, d)}{k}, \quad (31)$$

and the mean square displacement can be formulated as

$$\langle x(t)^2 \rangle = \frac{k_B T}{k} \left[1 - \exp\left(-\frac{2t}{\tau}\right) \right]. \quad (32)$$

For spheres with a radius of 500 nm and an optical trap with stiffness $k = 10, 1,$ and $0.1 \text{ pN}/\mu\text{m}$, the corresponding characteristic length squares for the autocorrelation function $\sqrt{k_B T/k}$ are approximately 20, 65, and 200 nm in a pure solvent. The corresponding decorrelation times are 1, 10, and 100 ms, respectively, whereas in a dilute polymer solution, the decorrelation times increases slightly to 1.33, 13.3, and 133 ms in a pure solvent. This increase is due to the enhanced viscous resistance or slower motion of the particles. Although the discussion here is applicable to an isolated particle, the resulting characteristic distribution length is about the same order of magnitude as the diffusive length (independent of hydrodynamic interactions) observed in Fig. 5(b) because the total simulation time (2 s) is far beyond the decorrelation time. In other words, the depletion effect shifts the probability distribution of the random walk instead of altering the characteristic diffusive length. If the bulk viscosity is used instead of the two-layer depletion model, the decorrelation times would be 1.53, 15.3, and 153 ms, respectively. One can speculate that these analysis for the result of stochastic motion of single sphere is applicable for colloid-polymer dispersions with colloid volume fraction $\ll 10^{-5}$ or an averaged pair separation distance $\gg 100a$.

In Fig. 6 results are shown for the random motion of a trapped single sphere. In Fig. 6(a) the mean square displacement is plotted versus time in a pure solvent and in polymer solutions with and without depletion. In Fig. 6(a), the thin blue curve is the ensemble average over 100 samples which is considerably noisy compared to the thick black curve from the average over 10^4 samples. Parameters applied to the simulations are: $a = 500 \text{ nm}$, $k = 10 \text{ pN}/\mu\text{m}$, $R_g/a = 1$, viscosity ratio $\lambda = 1.611$, depletion thickness $d/a = 0.638$ for the normalized polymer concentration $\epsilon = 0.5$, and the time step for the Brownian simulation $\Delta t = 3 \times 10^{-5} \text{ s}$. The data points obtained from Eqs. (30) and (32) agree well with the Brownian simulations. The sample size for computing the

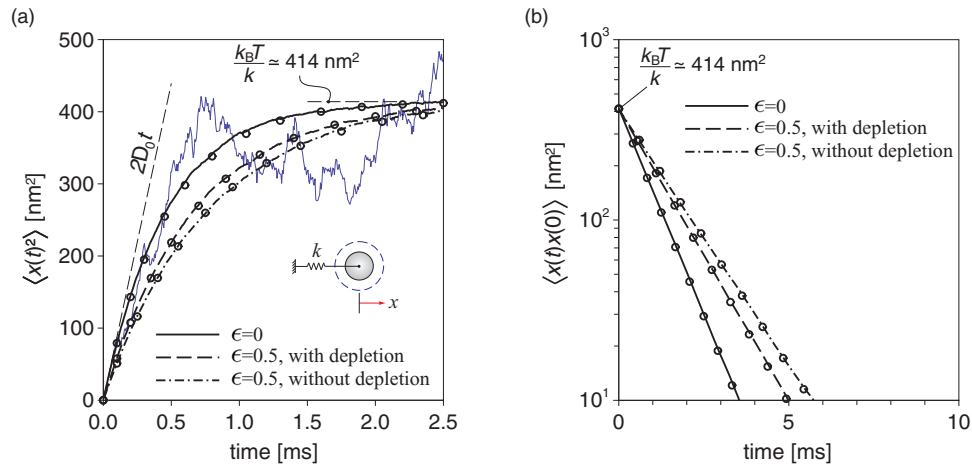


FIG. 6. Brownian simulation results for a single sphere showing the mean square displacement versus time (a) and the autocorrelation function (b) of the random motion of the isolated sphere in pure solvent ($\epsilon = 0$) and dilute polymer solution ($\epsilon = 0.5$) with and without the polymer depletion effect under ambient temperature. The thin blue curve is the average from 100 samples ($\epsilon = 0$), and the thick continuous curve is the result from averaging over 10^4 samples. Data points represent the analytical solutions from Eqs. (30) and (32).

autocorrelation function is sufficiently large by considering total simulation time around 10 s. The decay time can be obtained from the best fit to the numerical results based on the exponential decay given by Eq. (31). The computed versus analytical decay times are 0.9424, 1.3298, and 1.5183 ms for $\epsilon = 0$, $\epsilon = 0.5$ with depletion, and $\epsilon = 0.5$ without depletion, respectively. Under the same stiffness, the large viscous effect essentially increases the decorrelation time. At shorter times the difference is negligible, whereas at longer times the viscous effect enhances the autocorrelation along the harmonic force direction as expected. Therefore, the case without the depletion effect has the largest decorrelation time (and thus the g factor) due to the highest viscous resistance.

For the pair interaction, the analytical pair correlation function of spheres in homogeneous fluids is available.^{34,35} A straightforward extension of this result to incorporate the depletion effect for the two-dimensional movement of a pair of spheres in x – and z – direction (y and z are equivalent) can be written as

$$\begin{bmatrix} \dot{x}_1 \\ \dot{z}_1 \\ \dot{x}_2 \\ \dot{z}_2 \end{bmatrix} = \begin{bmatrix} 1 + A^s & 0 & A^c & 0 \\ 0 & 1 + B^s & 0 & B^c \\ A^c & 0 & 1 + A^s & 0 \\ 0 & B^c & 0 & 1 + B^s \end{bmatrix} \times \begin{bmatrix} -kx_1 - F^{\text{dep}} + F_1^{\text{B}} \\ -kz_1 + F_1^{\text{B}} \\ -kx_2 + F^{\text{dep}} + F_2^{\text{B}} \\ -kz_2 + F_2^{\text{B}} \end{bmatrix} / (6\pi\eta_s a g_0). \quad (33)$$

The eigenvalues of the mobility tensor are $1/6\pi\eta_s a g_{\parallel}^{\text{I}}$, $1/6\pi\eta_s a g_{\parallel}^{\text{II}}$, $1/6\pi\eta_s a g_{\perp}^{\text{I}}$, and $1/6\pi\eta_s a g_{\perp}^{\text{II}}$, which represent the inverse hydrodynamic resistance in the four hydrodynamic modes with boundary conditions described in Eq. (22). The four principal vectors are $Y_{\parallel}^{\text{I}} = x_1 + x_2$, $Y_{\parallel}^{\text{II}} = x_1 - x_2$, $Y_{\perp}^{\text{I}} = z_1 + z_2$, and $Y_{\perp}^{\text{II}} = z_1 - z_2$, representing the common (collective, mode I) and relative (mode II) motions

of spheres in both parallel and perpendicular directions, respectively. The eigenvectors lead to the following autocorrelation functions for the pair interactions under the four eigenmodes,

$$\begin{aligned} \langle Y_{\parallel}^{\text{I}}(t) Y_{\parallel}^{\text{I}}(0) \rangle &= \frac{2k_B T}{k} \left[\exp\left(-\frac{t}{\tau_{\parallel}^{\text{I}}}\right) \right], \\ \langle Y_{\parallel}^{\text{II}}(t) Y_{\parallel}^{\text{II}}(0) \rangle &= \left(\frac{2F^{\text{dep}}}{k}\right)^2 + \frac{2k_B T}{k} \left[\exp\left(-\frac{t}{\tau_{\parallel}^{\text{II}}}\right) \right], \\ \langle Y_{\perp}^{\text{I}}(t) Y_{\perp}^{\text{I}}(0) \rangle &= \frac{2k_B T}{k} \left[\exp\left(-\frac{t}{\tau_{\perp}^{\text{I}}}\right) \right], \quad \text{and} \quad (34) \\ \langle Y_{\perp}^{\text{II}}(t) Y_{\perp}^{\text{II}}(0) \rangle &= \frac{2k_B T}{k} \left[\exp\left(-\frac{t}{\tau_{\perp}^{\text{II}}}\right) \right], \end{aligned}$$

where the individual decay time for each mode are $\tau_{\parallel}^{\text{I}} = 6\pi\eta_s g_{\parallel}^{\text{I}}/k$, $\tau_{\parallel}^{\text{II}} = 6\pi\eta_s g_{\parallel}^{\text{II}}/k$, $\tau_{\perp}^{\text{I}} = 6\pi\eta_s g_{\perp}^{\text{I}}/k$, and $\tau_{\perp}^{\text{II}} = 6\pi\eta_s g_{\perp}^{\text{II}}/k$. The four decay times of the corresponding principal modes all reduce to the single particle limit as the separation distance becomes large, e.g., $r/a > \mathcal{O}(10^2)$. Figure 7 demonstrates autocorrelation functions under the four principal modes with various concentration and separation distance. Comparing Figs. 7(a) with 7(b), and 7(c) with 7(d), in both directions the decorrelation times in mode I (the collective motion, Figs. 7(a) and 7(c)) are always shorter than mode II (relative motion, Figs. 7(b) and 7(d)). The reason is because the hydrodynamic resistance is always higher in the relative motion, which slows down the particle motion more significantly especially in the lubrication regime. When comparing parallel to perpendicular motions, in mode I the behavior is similar for both motions because the depletion effect has been canceled in both eigenmodes Y_{\parallel}^{I} and Y_{\perp}^{I} and therefore only the hydrodynamic effect plays a role in mode I, in which the correction factors in parallel and

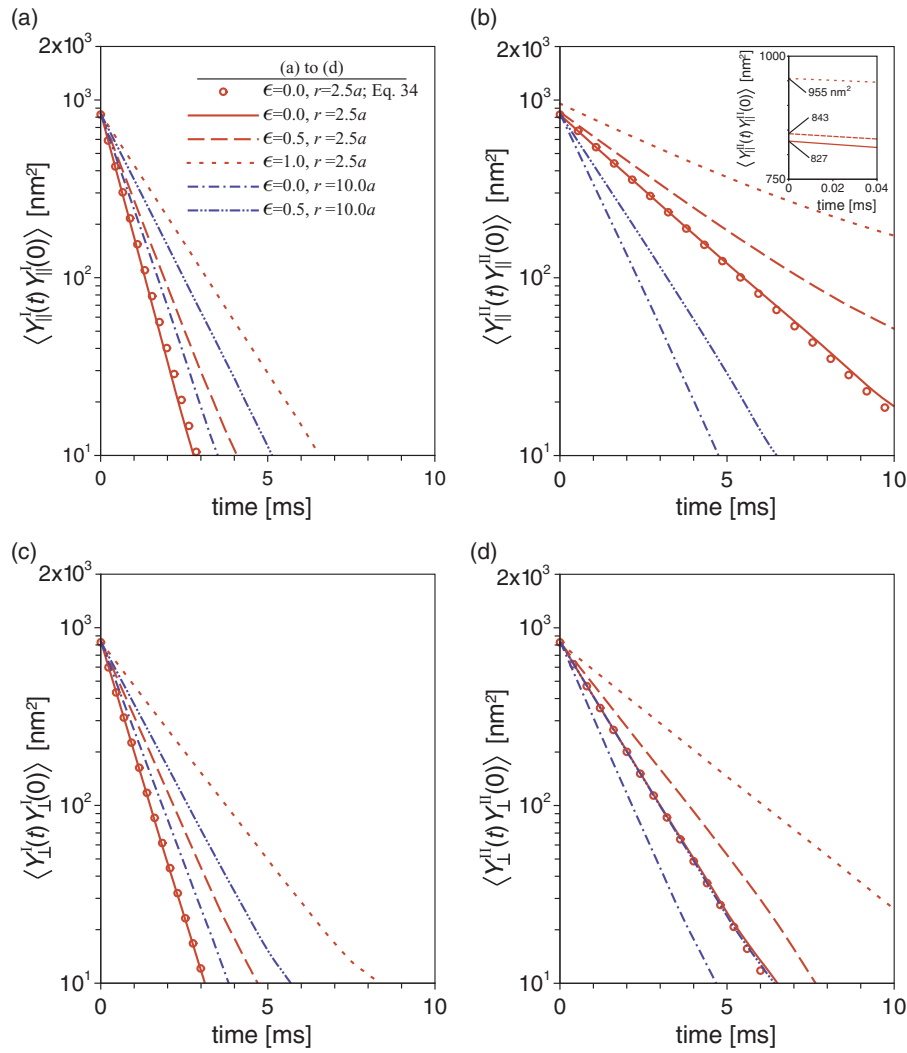


FIG. 7. (a)–(d) Autocorrelation functions of the displacement along the four principal directions. The data points represent the analytical results (Eq. (34)) using the mobility functions given by Batchelor.⁴⁷ Parameters for particles and polymer are the same as in Fig. 6.

perpendicular motions have similar values. In the eigenmode II parallel motion (Fig. 7(b)), the autocorrelation function includes the decomposed contributions from two sources, the depletion force and the hydrodynamic resistance. The polymer depletion effect changes the equilibrium position of spheres along $Y_{||}^{\text{II}}$ direction with a magnitude of $2F^{\text{dep}}/k$. This shifts the autocorrelation of spheres' movement in parallel mode II with a magnitude of $4(F^{\text{dep}}/k)^2$. In nearby location of optical traps ($r/a \simeq 2.5$) the decorrelation time of motion of spheres is enhanced. In mode II, the increase of the decorrelation time is more pronounced in parallel (Fig. 7(b)) than in the perpendicular (Fig. 7(d)) directions. It is due to the larger hydrodynamic correction factor $g_{||}^{\text{II}}$ compared to g_{\perp}^{II} , which can be speculated from the g -factor plots (Figs. 4(b) and 4(c)). With increasing polymer concentration ϵ the decorrelation time in all modes will increase due to larger viscous resistance force. In principle, one may compute the g factor and the decay time of displacement autocorrelation functions in four principal directions by experimentally measuring the auto- and cross-correlation of displacements. It is also valuable to validate the attractive potential between two hard spheres from the dynamic

view point through the shift $4(F^{\text{dep}}/k)^2$ in the autocorrelation function ($Y_{||}^{\text{II}}$).

In physical space, the correlation functions on the x, z plane are

$$\begin{aligned}
 \langle x_1(t)x_1(0) \rangle &= \left(\frac{F^{\text{dep}}}{k} \right)^2 + \frac{k_B T}{2k} \left[\exp\left(-\frac{t}{\tau_{||}^{\text{I}}}\right) + \exp\left(-\frac{t}{\tau_{||}^{\text{II}}}\right) \right], \\
 \langle x_1(t)x_2(0) \rangle &= -\left(\frac{F^{\text{dep}}}{k} \right)^2 + \frac{k_B T}{2k} \left[\exp\left(-\frac{t}{\tau_{||}^{\text{I}}}\right) - \exp\left(-\frac{t}{\tau_{||}^{\text{II}}}\right) \right], \\
 \langle z_1(t)z_1(0) \rangle &= \frac{k_B T}{2k} \left[\exp\left(-\frac{t}{\tau_{\perp}^{\text{I}}}\right) + \exp\left(-\frac{t}{\tau_{\perp}^{\text{II}}}\right) \right], \quad \text{and} \\
 \langle z_1(t)z_2(0) \rangle &= \frac{k_B T}{2k} \left[\exp\left(-\frac{t}{\tau_{\perp}^{\text{I}}}\right) - \exp\left(-\frac{t}{\tau_{\perp}^{\text{II}}}\right) \right].
 \end{aligned} \tag{35}$$

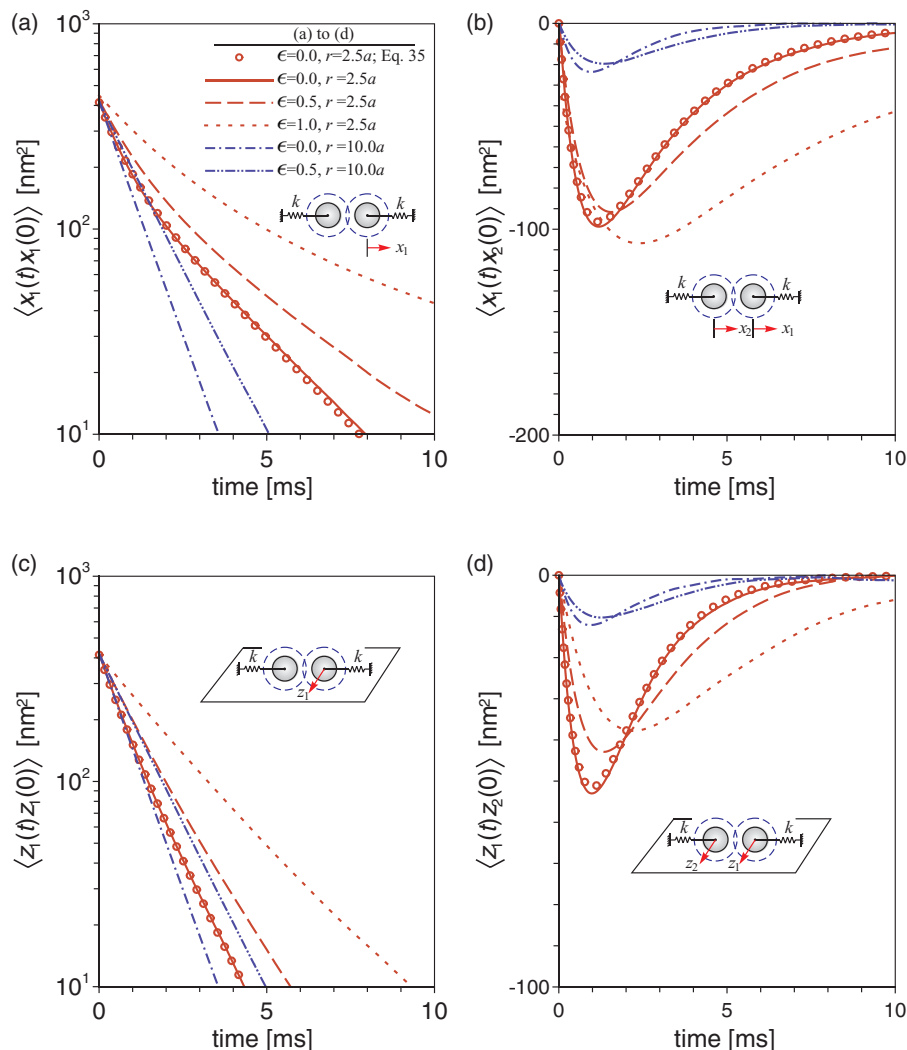


FIG. 8. (a)–(d) Correlation functions of the displacement of two trapped spheres in the xz -plane under the influence of depletion layers. Parameters used for particles and polymer conditions are the same as in Fig. 6.

The correlation results are plotted in Fig. 8. Note that correlation functions above include the self- and cross-correlations in the principle directions, and can be computed by

$$\begin{aligned} \langle x_1(t)x_1(0) \rangle &= \frac{1}{4} [\langle Y_{\parallel}^I(t)Y_{\parallel}^I(0) \rangle + \langle Y_{\parallel}^I(t)Y_{\parallel}^{II}(0) \rangle \\ &\quad + \langle Y_{\parallel}^I(0)Y_{\parallel}^{II}(t) \rangle + \langle Y_{\parallel}^{II}(t)Y_{\parallel}^{II}(0) \rangle], \end{aligned} \quad (36)$$

and

$$\begin{aligned} \langle x_1(t)x_2(0) \rangle &= \frac{1}{4} [\langle Y_{\parallel}^I(t)Y_{\parallel}^I(0) \rangle - \langle Y_{\parallel}^I(t)Y_{\parallel}^{II}(0) \rangle \\ &\quad + \langle Y_{\parallel}^I(0)Y_{\parallel}^{II}(t) \rangle - \langle Y_{\parallel}^{II}(t)Y_{\parallel}^{II}(0) \rangle]. \end{aligned} \quad (37)$$

The same formulations are applied to find the correlations functions in the z -direction. Along the parallel direction (Figs. 8(a) and 8(b)) the auto- and cross-correlation functions at $t = 0$ deviates from $k_B T/k$ (auto) and zero (cross) with an amount of $(F^{\text{dep}}/k)^2$, however, the two decorrelation time scales involved maybe difficult to distinguish from each other. Similarly in the perpendicular direction, the correlation functions are determined by two time scales that originate from the

two hydrodynamic modes. Considering the decayed hydrodynamic interactions, at very long lag time all correlations vanish, while at zero lag time the cross-correlation vanishes, implying that apparently the particle does not feel the presence of another particle at the beginning due to the mutual cancellation of collective and relative motions. The entropic force has a finite influence on both correlations. They are always anti-correlated because the first mode (collective motion) always decays faster than the second mode (relative motion) due to its less resistance. In other words, this relative motion dominates the relevance of the displacements of both particles after certain lag time, and the pair interaction behaves like in its second or anticorrelated mode. This fact is not to be confused with the intuition obtained from a steady mobility analysis.

The largest anticorrelation appears at

$$t_{\min, \parallel} = \frac{\tau_{\parallel}^I \tau_{\parallel}^{II}}{\tau_{\parallel}^I - \tau_{\parallel}^{II}} \ln \left(\frac{\tau_{\parallel}^I}{\tau_{\parallel}^{II}} \right) = \frac{g_{\parallel}^I g_{\parallel}^{II}}{g_{\parallel}^I - g_{\parallel}^{II}} \ln \left(\frac{g_{\parallel}^I}{g_{\parallel}^{II}} \right). \quad (38)$$

The same formulation is applicable for the perpendicular direction. The depth of the anticorrelation in parallel direction

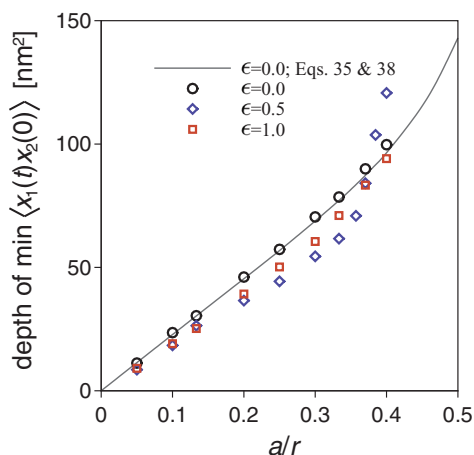


FIG. 9. The maximum value of the anticorrelation in the parallel direction versus the center-to-center separation distance. The limit $a/r = 0$ indicates an isolated particle, while $a/r = 0.5$ means both particles are in contact with each other. The reference curve is the analytical approximation based on the mobility function for the solvent-only case.

versus the distance of optical traps is predicted in Fig. 9. At large separation distance the motion obviously is uncorrelated. At short separation distance, the increase of the depth is due to both hydrodynamic and depletion interactions. Without the depletion effect, the analytical results from Batchelor's approximation (solid curves) is somewhat higher than the numerical simulation (black circles) because the approximation yields a relative lower lubrication force, which enhances the influence of the relative motion. Consistent results are shown by the two blue lines in Figs. 8(b) and 8(d), in which the higher viscosity gives a shallower anticorrelation. By bringing the pair particles closer to each other, the minimum value for $\langle x_1(t)x_2(0) \rangle$ is lower at small a/r and then higher for the polymer solution cases with depletion effect (red squares and blue diamonds) compared with the solvent-only case (black circles). The overlapping of the depletion zones appears at $a/r \approx 0.31$ ($\epsilon = 0.5$) and $a/r \approx 0.38$ ($\epsilon = 1.0$). Without depletion zones, the uniform polymer solution case, the hydrodynamic resistance experience by the spheres is higher because the higher bulk viscosity simply gives a shallower anticorrelation. Into the overlap region, the

entropic force brings particles toward each other and enhances anticorrelation mode. This effect is further enhanced by bringing the spheres closer. The complicated flow pattern and resistance in the two-layer model has relatively much less contribution compared with the entropic effect on the anticorrelation depth. Experimental validation is needed to validate this result.

It is interesting to see whether the proposed model can reproduce the statistical characteristics observed experimentally by using optical tweezers to measure the force between two hard-sphere like silica spheres in an aqueous solution containing long semiflexible DNA polymers by Verma *et al.*^{16,17} We simulate the corresponding dynamic trajectories and the equilibrium state of the effective pair interaction between two spheres in a polymer solution. Following the reported experimental conditions, the sphere radius is 625 nm, and DNA polymer radius of gyration is 500 nm. The stiffness of the optical traps is set to 0.3 pN/ μm in the simulation. The weak optical trap allows the particles to diffuse to an average distance $(k_B T/k)^{1/2}$ of about 117 nm, which is similar to the apparent thickness of the depletion layer. In our simulation under a good solvent condition, the positions of the random walks are tracked from the histogram so that the pair probability distribution $P^{\text{total}}(r)$ can be determined, which represents the probability of finding two spheres at certain center-to-center distance away from each other. The interaction potentials $W^{\text{total}}(r)$ that includes the contributions of depletion and optical traps is connected to the pair distribution through the Boltzmann relation, $P^{\text{total}}(r) \propto \exp(-W^{\text{total}}/k_B T)$. To subtract the trapping effect, a similar run is carried out without polymer so that $P^{\text{trap}}(r) \propto \exp(-W^{\text{trap}}/k_B T)$. The depletion potential therefore can be obtained from $W^{\text{dep}}(r) = k_B T \ln[P^{\text{trap}}(r)/P^{\text{total}}(r)] - C$, where C can be a fitting constant or can be determined from the proportionality constants from both probability distributions. In Fig. 10 we compare the modeling results with experimental data of Verma *et al.*^{16,17} Overall the results are in good agreement with experiment, indicating that the simulation of our model has correctly reproduced the stochastic dynamics of the particles in the long-time regime. As expected the model agrees well with the experimental data in the dilute regime (Fig. 10(a)). Relatively noisy simulation data appear at small separation

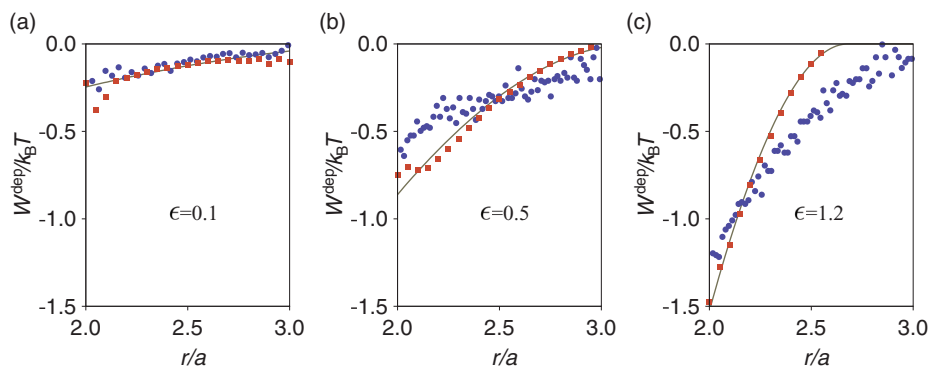


FIG. 10. (a)–(c) The depletion potential between two hard spheres in non-adsorbing polymer solution for $\epsilon = 0.1, 0.5$, and 1.2 , corresponding to the extracted experimental data $5 \mu\text{g/ml}$, $25 \mu\text{g/ml}$, and $120 \mu\text{g/ml}$,¹⁶ respectively. The solid lines are from the AOV model (Eq. (3)), red squares are Brownian simulation results that reproduce the dynamic process, and blue dots are redrawn experimental data from Verma *et al.*^{16,17} The colloid radius is 625 nm, polymer radius of gyration is 500 nm, spring constant $k = 0.3 \text{ pN}/\mu\text{m}$, and the distance between traps is $2.5a$. The simulation time is 18.5 min with time step 5.5 ms.

distance due to the relatively less samples within the time duration. In cases (b) and (c) with higher polymer concentration, the two-layer model overpredicts the strength of the depletion potential. Since the experimental data are model independent, the deviation between modeling and experiment is more likely due to the simplified thermodynamic potential we have applied. Furthermore, at equilibrium, our simulation including AO and hydrodynamic interactions almost recover the AO-only result, implying that in this comparison hydrodynamic interactions is indeed negligible in approximating $P(r)$ using the Boltzmann relation. With the help of dynamic simulation, it is also possible to extract the equilibrium depletion information from the eigen-decomposition of the correlation functions presented above.

Finally, there are thermodynamic and hydrodynamic concerns about the accuracy of the two-layer model presented here. Established equilibrium models on predicting depletion forces include AO, phantom sphere free volume, mean field, and the polymer reference interaction site models.^{6,7,10,30,55} The AO and mean field models predict the depletion potential accurately for small polymers in the dilute limit, however, they overpredict the depth of the potential when the polymer concentration is beyond the overlapping regime and when the polymer chain is no longer much smaller than the colloid.^{20,21} Similar results were also found for rod-shaped depletants.^{56–58} However, in principle, without changing the modeling framework, various depletion models that take mean-field or PRISM into account may be casted into the proposed dynamic model in terms of an effective depletion thickness derived from a more detailed theory. Further comparison and validation are needed. The second concern is regarding the mobility analysis. We have investigated the accuracy of the two-layer approach previously.^{27,59} The finding is that the mean field approach overestimates the attractive potential when $R_g \sim a$. This is consistent with the results found in Fig. 10. Comparing with the simulation results and AO model, the experimental data have a shallower potential close to the colloidal surface. The difference is likely due to an increase probability of existence of polymer chains near the colloidal surface as the polymer concentration increases, and thus the translational entropy (depletion) effect becomes weaker. For polymer concentrations beyond the overlap concentration the two-layer model is accurate for $R_g < a$. Our choice of making the calculations for $R_g \sim a$ is to compare with available experimental data.¹⁶ Furthermore, the primitive two-layer model significantly simplifies the three-dimensional computation to reveal the dynamic characteristics on pair-correlated motions.

IV. CONCLUSION

We presented a theoretical description that enables to characterize the stochastic motions of a pair of hard spheres in non-adsorbing polymer solutions. Based on a two-layer approximation for the polymer depletion effect, the hydrodynamic mobility tensor is resolved by the boundary integral analysis, which determines the corresponding time evolution of stochastic displacements that are consistent with the fluctuation-dissipation theorem. We first find that the pres-

ence of depletion zones significantly modifies the hydrodynamic interactions between two moving spheres. Polymer depletion is found to distort the probability distribution of the random walks of two trapped spheres. The resulting auto- and cross-correlation functions are presented in the principal modes, which clearly identify the decomposed entropic and hydrodynamic effects on the dynamic behavior of two hard spheres under the influence of added polymers to the solvent for various particle separation distances. In the presence of depletants, the cross-correlation of the particle displacements is weakened in a way that higher viscosity slows down the motion significantly and lengthens the hydrodynamic decay time. However, the appearance of the depletion zone reduces this viscous effect. Finally, the cross-correlation is significantly enhanced when the depletion zones overlap.

ACKNOWLEDGMENTS

M. Karzar-Jeddi and T.-H. Fan acknowledge the support from NSF CMMI-0952646, R. Tuinier thanks DSM for support, and T. Taniguchi acknowledges the support from JSPS KAKENHI Grant No. 23340121.

APPENDIX: DIVERGENCE OF DIFFUSIVITIES

The divergence of the self diffusivity (Eqs. (12) and (13)) can be expressed as

$$\begin{aligned} \frac{\partial}{\partial \mathbf{r}_\alpha} \cdot \mathbf{D}_{\alpha\alpha} = & \frac{D_0}{g_0} \left[\frac{\mathbf{r}_{\alpha\beta} \mathbf{r}_{\alpha\beta}}{r^2} \cdot \frac{\partial A^s}{\partial \mathbf{r}_\alpha} + \left(\mathbf{I} - \frac{\mathbf{r}_{\alpha\beta} \mathbf{r}_{\alpha\beta}}{r^2} \right) \cdot \frac{\partial B^s}{\partial \mathbf{r}_\alpha} \right. \\ & + (A^s - B^s) \mathbf{r}_{\alpha\beta} \mathbf{r}_{\alpha\beta} \cdot \frac{\partial}{\partial \mathbf{r}_\alpha} \left(\frac{1}{r^2} \right) \\ & \left. + \left(\frac{A^s - B^s}{r^2} \right) \frac{\partial}{\partial \mathbf{r}_\alpha} \cdot (\mathbf{r}_{\alpha\beta} \mathbf{r}_{\alpha\beta}) \right], \quad (\text{A1}) \end{aligned}$$

where $\alpha, \beta = 1, 2$ and $\alpha \neq \beta$, $\mathbf{r}_{\alpha\beta} = \mathbf{r}_\beta - \mathbf{r}_\alpha$, and $r = |\mathbf{r}_\beta - \mathbf{r}_\alpha|$. By simplifying the differential terms on the right where

$$\begin{aligned} \frac{\partial}{\partial \mathbf{r}_\alpha} \cdot \mathbf{D}_{\alpha\alpha} = & \frac{D_0}{g_0} \left\{ \frac{\mathbf{r}_{\alpha\beta} \mathbf{r}_{\alpha\beta}}{r^2} \cdot \left(\frac{-\mathbf{r}_{\alpha\beta}}{r} \frac{\partial A^s}{\partial r} \right) \right. \\ & + \left(\mathbf{I} - \frac{\mathbf{r}_{\alpha\beta} \mathbf{r}_{\alpha\beta}}{r^2} \right) \cdot \left(\frac{-\mathbf{r}_{\alpha\beta}}{r} \frac{\partial B^s}{\partial r} \right) \\ & + (A^s - B^s) \mathbf{r}_{\alpha\beta} \mathbf{r}_{\alpha\beta} \cdot \left(\frac{2\mathbf{r}_{\alpha\beta}}{r^4} \right) \\ & \left. + \frac{A^s - B^s}{r^2} \left[-\mathbf{r}_{\alpha\beta} \cdot \mathbf{I} + \mathbf{r}_{\alpha\beta} \left(\frac{\partial}{\partial \mathbf{r}_\alpha} \cdot \mathbf{r}_{\alpha\beta} \right) \right] \right\} \\ = & \frac{D_0}{g_0} \left[\frac{-r^2 \mathbf{r}_{\alpha\beta}}{r^3} \frac{\partial A^s}{\partial r} + \frac{-\mathbf{r}_{\alpha\beta}}{r} \frac{\partial B^s}{\partial r} + \frac{r^2 \mathbf{r}_{\alpha\beta}}{r^3} \frac{\partial B^s}{\partial r} \right. \\ & \left. + \frac{2(A^s - B^s)}{r^2} \mathbf{r}_{\alpha\beta} + \frac{-4(A^s - B^s)}{r^2} \mathbf{r}_{\alpha\beta} \right]. \quad (\text{A2}) \end{aligned}$$

Therefore,

$$\frac{\partial}{\partial \mathbf{r}_\alpha} \cdot \mathbf{D}_{\alpha\alpha} = \frac{-D_0}{g_0} \left[\frac{\partial A^s}{\partial r} + \frac{2(A^s - B^s)}{r} \right] \frac{\mathbf{r}_{\alpha\beta}}{r}. \quad (\text{A3})$$

Similarly, the divergence of the mutual diffusivity can be expressed as

$$\begin{aligned} \frac{\partial}{\partial \mathbf{r}_\beta} \cdot \mathbf{D}_{\alpha\beta} = & \frac{D_0}{g_0} \left[\frac{\mathbf{r}_{\alpha\beta} \mathbf{r}_{\alpha\beta}}{r^2} \cdot \left(\frac{\mathbf{r}_{\alpha\beta}}{r} \frac{\partial A^c}{\partial r} \right) \right. \\ & + \left(\mathbf{I} - \frac{\mathbf{r}_{\alpha\beta} \mathbf{r}_{\alpha\beta}}{r^2} \right) \cdot \left(\frac{\mathbf{r}_{\alpha\beta}}{r} \frac{\partial B^c}{\partial r} \right) \\ & + (A^c - B^c) \mathbf{r}_{\alpha\beta} \mathbf{r}_{\alpha\beta} \cdot \left(\frac{-2\mathbf{r}_{\alpha\beta}}{r^4} \right) + \frac{A^c - B^c}{r^2} \\ & \left. \times \left[\mathbf{r}_{\alpha\beta} \cdot \mathbf{I} + \mathbf{r}_{\alpha\beta} \left(\frac{\partial}{\partial \mathbf{r}_\beta} \cdot \mathbf{r}_{\alpha\beta} \right) \right] \right], \quad (\text{A4}) \end{aligned}$$

which simplifies to Eq. (19),

$$\frac{\partial}{\partial \mathbf{r}_\beta} \cdot \mathbf{D}_{\alpha\beta} = \frac{D_0}{g_0} \left[\frac{\partial A^c}{\partial r} + \frac{2(A^c - B^c)}{r} \right] \frac{\mathbf{r}_{\alpha\beta}}{r}. \quad (\text{A5})$$

In a uniform fluid ($\lambda=1$), $A^s=B^s=0$, $A^c=3a/2r$, $B^c=3a/4r$ for the Oseen tensor, and $A^s=B^s=0$, $A^c=3a/2r - a^3/r^3$, $B^c=3a/4r + a^3/2r^3$ for Rotne-Prager tensor. It is known that above divergences vanish, which very much simplifies the simulation.

- ¹S. B. Zimmerman and A. P. Minton, "Macromolecular crowding: biochemical, biophysical, and physiological consequences," *Annu. Rev. Biophys. Biomol. Struct.* **22**(1), 27–65 (1993).
- ²R. J. Ellis and A. P. Minton, "Join the crowd," *Nature* **425**, 27–28 (2003).
- ³J.-L. Doublier, C. Garnier, D. Renard, and C. Sanchez, "Protein-polysaccharide interactions," *Curr. Opin. Colloid Interface Sci.* **5**(3), 202–214 (2000).
- ⁴S. Tanaka and M. Ataka, "Protein crystallization induced by polyethylene glycol: A model study using apoferritin," *J. Chem. Phys.* **117**(7), 3504–3510 (2002).
- ⁵L. Rossi, S. Sacanna, W. T. M. Irvine, P. M. Chaikin, D. J. Pine, and A. P. Philipse, "Cubic crystals from cubic colloids," *Soft Matter* **7**(9), 4139–4142 (2011).
- ⁶S. Asakura and F. Oosawa, "On interaction between two bodies immersed in a solution of macromolecules," *J. Chem. Phys.* **22**, 1255–1256 (1954).
- ⁷S. Asakura and F. Oosawa, "Interaction between particles suspended in solutions of macromolecules," *J. Polym. Sci.* **33**(126), 183–192 (1958).
- ⁸A. Vrij, "Polymers at interfaces and the interactions in colloidal dispersions," *Pure Appl. Chem.* **48**(4), 471–483 (1976).
- ⁹A. P. Gast, C. K. Hall, and W. B. Russel, "Polymer-induced phase separations in nonaqueous colloidal suspensions," *J. Colloid Interface Sci.* **96**(1), 251–267 (1983).
- ¹⁰H. N. W. Lekkerkerker, W. C.-K. Poon, P. N. Pusey, A. Stroobants, and P. B. Warren, "Phase behaviour of colloid+polymer mixtures," *Europhys. Lett.* **20**(6), 559–564 (1992).
- ¹¹H. N. W. Lekkerkerker and A. Stroobants, "Phase behaviour of rod-like colloid + flexible polymer mixtures," *Il Nuovo Cimento* **16** D(8), 949–962 (1994).
- ¹²T. Koda and S. Ikeda, "Test of the scaled particle theory for aligned hard spherocylinders using monte carlo simulation," *J. Chem. Phys.* **116**(13), 5825–5830 (2002).
- ¹³W. C. K. Poon, "The physics of a model colloid–polymer mixture," *J. Phys.: Condens. Matter* **14**(33), R859–R880 (2002).
- ¹⁴G. J. Fleer and R. Tuinier, "Analytical phase diagrams for colloids and non-adsorbing polymer," *Adv. Colloid Interface Sci.* **143**(1), 1–47 (2008).
- ¹⁵R. Tuinier, J. K. G. Dhont, and T.-H. Fan, "How depletion affects sphere motion through solutions containing macromolecules," *Europhys. Lett.* **75**(6), 929–935 (2006).
- ¹⁶R. Verma, J. C. Crocker, T. C. Lubensky, and A. G. Yodh, "Entropic colloidal interactions in concentrated DNA solutions," *Phys. Rev. Lett.* **81**(18), 4004–4007 (1998).
- ¹⁷R. Verma, J. C. Crocker, T. C. Lubensky, and A. G. Yodh, "Attractions between hard colloidal spheres in semiflexible polymer solutions," *Macromolecules* **33**(1), 177–186 (2000).
- ¹⁸M. Fuchs and K. S. Schweizer, "Structure of colloid-polymer suspensions," *J. Phys.: Condens. Matter* **14**(12), R239–R269 (2002).
- ¹⁹J. Dzubiella, C. N. Likos, and H. Löwen, "Phase behavior and structure of star-polymer–colloid mixtures," *J. Chem. Phys.* **116**(21), 9518–9530 (2002).
- ²⁰S. A. Shah, Y.-L. Chen, K. S. Schweizer, and C. F. Zukoski, "Phase behavior and concentration fluctuations in suspensions of hard spheres and nearly ideal polymers," *J. Chem. Phys.* **118**(7), 3350–3361 (2003).
- ²¹Y.-L. Chen, K. S. Schweizer, and M. Fuchs, "Phase separation in suspensions of colloids, polymers and nanoparticles: Role of solvent quality, physical mesh, and nonlocal entropic repulsion," *J. Chem. Phys.* **118**(8), 3880–3890 (2003).
- ²²K. J. Mutch, J. S. van Duijneveldt, and J. Eastoe, "Colloid–polymer mixtures in the protein limit," *Soft Matter* **3**(2), 155–167 (2007).
- ²³D. Kleshchanok, R. Tuinier, and P. R. Lang, "Direct measurements of polymer-induced forces," *J. Phys.: Condens. Matter* **20**(7), 073101 (2008).
- ²⁴E. Donath, A. Krabi, M. Nirschl, V. M. Shilov, M. I. Zharkikh, and B. Vincent, "Stokes friction coefficient of spherical particles in the presence of polymer depletion layers. Analytical and numerical calculations, comparison with experimental data," *J. Chem. Soc. Faraday Trans.* **93**(1), 115–119 (1997).
- ²⁵R. Tuinier and T. Taniguchi, "Polymer depletion-induced slip near an interface," *J. Phys.: Condens. Matter* **17**(2), L9–L14 (2005).
- ²⁶T.-H. Fan, J. K. G. Dhont, and R. Tuinier, "Motion of a sphere through a polymer solution," *Phys. Rev. E* **75**(1), 011803 (2007).
- ²⁷T.-H. Fan, B. Xie, and R. Tuinier, "Asymptotic analysis of tracer diffusivity in nonadsorbing polymer solutions," *Phys. Rev. E* **76**(5), 051405 (2007).
- ²⁸R. Tuinier and T.-H. Fan, "Scaling of nanoparticle retardation in semi-dilute polymer solutions," *Soft Matter* **4**, 254–257 (2008).
- ²⁹T.-H. Fan and R. Tuinier, "Hydrodynamic interaction of two colloids in nonadsorbing polymer solutions," *Soft Matter* **6**(3), 647–654 (2010).
- ³⁰G. J. Fleer, A. M. Skvortsov, and R. Tuinier, "Mean-field equation for the depletion thickness," *Macromolecules* **36**(20), 7857–7872 (2003).
- ³¹A. Ashkin, J. M. Dziedzic, J. E. Bjorkholm, and S. Chu, "Observation of a single-beam gradient force optical trap for dielectric particles," *Opt. Lett.* **11**(5), 288–290 (1986).
- ³²J. C. Crocker and D. G. Grier, "Microscopic measurement of the pair interaction potential of charge-stabilized colloid," *Phys. Rev. Lett.* **73**(2), 352–355 (1994).
- ³³J. C. Crocker, "Measurement of the hydrodynamic corrections to the Brownian motion of two colloidal spheres," *J. Chem. Phys.* **106**, 2837–2840 (1997).
- ³⁴J.-C. Meiners and S. R. Quake, "Direct measurement of hydrodynamic cross correlations between two particles in an external potential," *Phys. Rev. Lett.* **82**(10), 2211–2214 (1999).
- ³⁵P. Bartlett, S. I. Henderson, and S. J. Mitchell, "Measurement of the hydrodynamic forces between two polymer-coated spheres," *Philos. Trans. A: Math. Phys. Eng. Sci.* **359**(1782), 883–895 (2001).
- ³⁶M. Reichert and H. Stark, "Hydrodynamic coupling of two rotating spheres trapped in harmonic potentials," *Phys. Rev. E* **69**(3), 031407 (2004).
- ³⁷N. K. Metzger, R. F. Marchington, M. Mazilu, R. L. Smith, K. Dholakia, and E. M. Wright, "Measurement of the restoring forces acting on two optically bound particles from normal mode correlations," *Phys. Rev. Lett.* **98**(6), 068102 (2007).
- ³⁸A. Ziehl, J. Bammert, L. Holzer, C. Wagner, and W. Zimmermann, "Direct measurement of shear-induced cross-correlations of Brownian motion," *Phys. Rev. Lett.* **103**(23), 230602 (2009).
- ³⁹J. Bammert, L. Holzer, and W. Zimmermann, "Dynamics of two trapped Brownian particles: Shear-induced cross-correlations," *Eur. Phys. J. E* **33**(4), 313–325 (2010).
- ⁴⁰D.-H. He, T. Yang, W.-H. Li, Q.-L. Zhang, and H.-R. Ma, "Brownian dynamics simulation of two confined colloidal particles," *Chin. Phys.* **16**(10), 3138–3145 (2007).
- ⁴¹F. Rodriguez, "Graphical solution of the Martin equation," *J. Polym. Sci. Pol. Lett.* **11**(7), 485–486 (1973).
- ⁴²J. M. Deutch and I. Oppenheim, "Molecular theory of Brownian motion for several particles," *J. Chem. Phys.* **54**, 3547–3555 (1971).
- ⁴³R. Kubo, "The fluctuation-dissipation theorem," *Rep. Prog. Phys.* **29**(1), 255–284 (1966).
- ⁴⁴T. Tlusty, A. Meller, and R. Bar-Ziv, "Optical gradient forces of strongly localized fields," *Phys. Rev. Lett.* **81**(8), 1738–1741 (1998).

- ⁴⁵D. L. Ermak and J. A. McCammon, "Brownian dynamics with hydrodynamic interactions," *J. Chem. Phys.* **69**, 1352–1360 (1978).
- ⁴⁶J. Rotne and S. Prager, "Variational treatment of hydrodynamic interaction in polymers," *J. Chem. Phys.* **50**, 4831–4837 (1969).
- ⁴⁷G. K. Batchelor, "Brownian diffusion of particles with hydrodynamic interaction," *J. Fluid Mech.* **74**(1), 1–29 (1976).
- ⁴⁸J. K. G. Dhont, *An Introduction to Dynamics of Colloids* (Elsevier Science, 1996).
- ⁴⁹M. Stimson and G. B. Jeffery, "The motion of two spheres in a viscous fluid," *Proc. R. Soc. A* **111**(757), 110–116 (1926).
- ⁵⁰H. Brenner, "The slow motion of a sphere through a viscous fluid towards a plane surface," *Chem. Eng. Sci.* **16**(3), 242–251 (1961).
- ⁵¹M. E. O'Neill and S. R. Majumdar, "Asymmetrical slow viscous fluid motions caused by the translation or rotation of two spheres. Part I: The determination of exact solutions for any values of the ratio of radii and separation parameters," *Z. Angew. Math. Phys.* **21**(2), 164–179 (1970).
- ⁵²O. A. Ladyzhenskaya and R. A. Silverman, *The Mathematical Theory of Viscous Incompressible Flow* (Gordon and Breach, New York, 1969).
- ⁵³C. Pozrikidis, *Boundary Integral and Singularity Methods for Linearized Viscous Flow* (Cambridge University Press, 1992).
- ⁵⁴M. Doi and S. F. Edwards, *The Theory of Polymer Dynamics* (Oxford University Press, 1988).
- ⁵⁵K. S. Schweizer and J. G. Curro, "PRISM theory of the structure, thermodynamics, and phase transitions of polymer liquids and alloys," *Adv. Polym. Sci.* **116**, 319–377 (1994).
- ⁵⁶K. Yaman, C. Jeppesen, and C. M. Marques, "Depletion forces between two spheres in a rod solution," *Europhys. Lett.* **42**(2), 221–226 (1998).
- ⁵⁷K.-H. Lin, J. C. Crocker, A. C. Zeri, and A. G. Yodh, "Colloidal interactions in suspensions of rods," *Phys. Rev. Lett.* **87**(8), 088301 (2001).
- ⁵⁸Y.-L. Chen and K. S. Schweizer, "Liquid-state theory of structure, thermodynamics, and phase separation in suspensions of rod polymers and hard spheres," *J. Phys. Chem. B* **108**(21), 6687–6696 (2004).
- ⁵⁹R. Tuinier, J. K. G. Dhont, T. Taniguchi, and T.-H. Fan, "Nanoparticle retardation in semidilute polymer solutions," *AIP Conf. Proc.* **982**, 326–330 (2008).